

Arrest of the flow of wet granular matter

Klaus Roeller¹, Johannes Blaschke^{1,2}, Stephan Herminghaus^{1,2}
and Jürgen Vollmer^{1,2,†}

¹Max-Planck-Institut für Dynamik und Selbstorganisation (MPIDS), 37077 Göttingen, Germany

²Fakultät für Physik, Georg-August-Universität Göttingen, 37077 Göttingen, Germany

(Received 16 April 2013; revised 4 October 2013; accepted 30 October 2013;
first published online 6 December 2013)

We study the arrest of three-dimensional flow of wet granular matter subject to a sinusoidal external force and a gravitational field confining the flow in the vertical direction. The minimal strength of the external force that is required to keep the system in motion, i.e. the critical force, is determined by considering the balance of injected and dissipated power. This provides a prediction whose quality is demonstrated by a data collapse for an extensive set of event-driven molecular-dynamics simulations where we varied the system size, particle number, the energy dissipated upon rupturing capillary bridges, and the bridge length at which rupture occurs. The same approach also works for systems that are kept at a fixed density by confining walls. In both cases, this universal method provides the critical force irrespective of the flow profile, and without specifying the hydrodynamic equations.

Key words: complex fluids, granular media

1. Introduction

Sudden arrest of granular flows is a challenge to the theoretical description of granular flows in a hydrodynamic setting (Jaeger, Nagel & Behringer 1996; Kadanoff 1999; Silbert *et al.* 2001; Aranson & Tsimring 2006; Jop, Forterre & Pouliquen 2006; Borzsonyi & Ecke 2007; Forterre & Pouliquen 2008; Luding 2009; Schall & van Hecke 2010; Slotterback *et al.* 2012), as well as an important problem in the engineering sciences (GDR MiDi 2004). Its modelling involves two challenges: (*a*) appropriately incorporating the role of dissipation arising from the particle interactions into the framework of the balance equations underlying hydrodynamic transport equations; and (*b*) addressing the roles of shear stresses, of the spatial distribution of stress, and of yield stress in systems where the flow is spatially anisotropic.

Recent studies (Utter & Behringer 2008; Berardi *et al.* 2010; van Hecke 2010; Tordesillas *et al.* 2011) of granular systems with purely repulsive interactions put severe constraints on hydrodynamic descriptions of dense flows by pointing out a lack of scale separation of microscopic and relevant hydrodynamic time and length scales. Among other problems, this gives rise to a severe dependence of the effective material

† Email address for correspondence: juergen.vollmer@ds.mpg.de

properties on the preparation history (Lois *et al.* 2009). In contrast, hydrodynamic and continuum-mechanics considerations appear to provide a good description for granular systems where the hard-core collisions with restitution are augmented by (reversible) short-ranged attraction between particles (Trappe *et al.* 2001; Rognon *et al.* 2006, 2008). Arguably this is due to the separation of connectivity and rigidity percolation in response to attractive interactions (Lois, Blawdziewicz & O'Hern 2007, 2008). This idealization of the particle interactions (Pitois, Moucheron & Chateau 2000) applies as long as high-impact-velocity collisions with high capillary numbers dominate the dynamics (see Kantak, Hrenya & Davis 2009; Donahue, Hrenya & Davis 2010a for recent applications). On the other hand, recent experimental (Liao & Hsiao 2010; Zhang *et al.* 2010; Remy, Khinast & Glasser 2012; Slotterback *et al.* 2012) and numerical (Remy *et al.* 2012) work on slowly moving shear flow in dense granular systems clearly underlines the important impact of dissipation due to the hysteretic formation and breaking of capillary bridges. Rather than accounting for the finite restitution in collisions and assuming reversible attractive forces, the present work therefore takes a complementary point of view: we explore slow flows in wet systems where dissipation is arising solely from the hysteretic nature of the capillary interaction between the wetting liquid and the particles, i.e. it is due to the formation and rupturing of capillary bridges between particles (Herminghaus 2005; Mitarai & Nori 2006). The hard-core collisions are elastic.

Shear forces that drive the flow can be modelled in various forms. Experimentally studying shear forces in granular systems can be done, for instance, by constructing two counter-rotating cylindrical walls (see Liao & Hsiao 2010 and references therein), by constructing a specialized shear cell (Ren, Dijksman & Behringer 2011), or by exploring a flow down an inclined plane (Quartier *et al.* 2000; Andreotti & Douady 2001; Andreotti, Daerr & Douady 2002; Rahbari *et al.* 2009). Moreover, in numerical models it is convenient to induce shear flow by applying a cosine force field (Schulz, Schulz & Herminghaus 2003; Herminghaus 2005; Roeller, Vollmer & Herminghaus 2009; Rahbari *et al.* 2010). Similarly to the method of images, this may be used to mimic zero flow velocity at the positions envisioned for the walls.

Here, we will focus on the arrest of flow when the force driving the flow falls below a threshold value F_{ex} . Considerations based on a system of sheared disks at a fixed density (Rahbari *et al.* 2010) suggest that the critical force, F_{ex} , results from the power balance between the energy-injection rate resulting from particle motion in the external force field, and the dissipation rate accounting for the rupture of capillary bridges between the particles.

Surprisingly, we show in the following that the same approach also describes the arrest of flow in a three-dimensional system with constant pressure. The motion in the third dimension is constrained by a hard wall at the bottom and a gravitational field in the vertical direction (figure 1a). For external driving forces close to F_{ex} all particles accumulate at the bottom of the cell such that the packing density always lies slightly above random close packing.

This finding is quite remarkable since the setting of constant density (Rahbari *et al.* 2010) fundamentally differs from that of constant pressure: at high packing fraction, the constraint of constant density requires cooperative large-scale rearrangements when two particles pass each other. In contrast the constraint of constant pressure allows particles to pass each other with only local rearrangements. In spite of this considerable difference, the arrest of flow in both settings is obtained by an informed

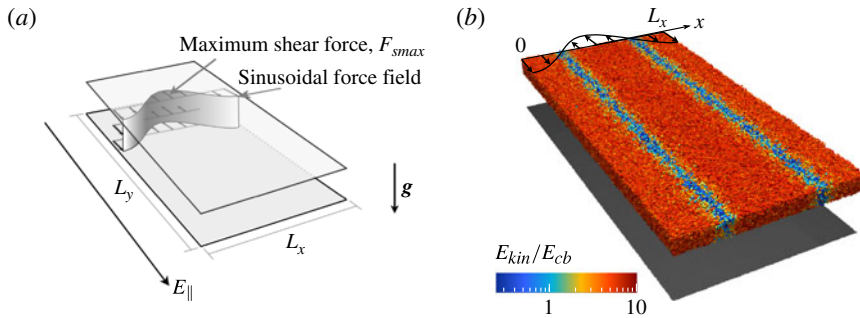


FIGURE 1. (Colour online) (a) Sketch of a system of width $L_x = L$ and length $L_y = 2L$ with periodic boundary conditions in the two lateral directions and elastically reflecting top and bottom plates. The space-dependent cosine-shaped force field is indicated by the vertical band and by arrows. Additionally, a gravitational force, \mathbf{g} , is acting downwards. (b) A snapshot of a simulation of 2.15×10^5 monodisperse spheres of diameter d that interact via a hysteretic square-well potential (see § 2.1). The cosine-shaped shear force field, $F_s(x)$, is sketched on top of the figure. The colour of each particle indicates its individual kinetic energy according to the colour bar at the bottom left. The system size is $L = 100d$ and $H = 12.5d$, and the filling height is $h = 8.8d$ for a shear force of amplitude $F_{smax} = 40 E_{cb}/L$, i.e. $\hat{F}_{smax} = 0.15$.

inspection of the global energy budget. We argue that this approach hence provides a versatile, universal method to study the arrest of granular flows.

Our paper is organized as follows. In § 2 we describe the system, our numerical approach, and the dimensionless units adopted for modelling. Subsequently, in § 3 we first provide a two-dimensional discussion of the power injected into the systems by the external field, and the dissipated power due to the breaking of capillary bridges and work against gravity. This power balance provides a prediction for the critical force F_{ex} . In § 4 the predicted parameter dependence of F_{ex} is compared to the numerical findings. Based on three scalar constants we describe the dependence of the stability boundary in the four-dimensional parameter space spanned by the system size L , the particle number N , the energy E_{cb} dissipated upon rupturing capillary bridges, and the critical bridge length s_{cb} where rupture occurs. (Here and in the following the subscript *cb* refers to capillary bridge.) The values of the three constants are interpreted and derived from the model in § 5. In § 6 we augment the two-dimensional model by flow features reflecting the vertical extent of the bed in order to calculate the numerical values of these constants.

2. The model

The system is confined in a rectangular cuboid of size $L \times 2L \times H$ with periodic boundary conditions in the x - and y -directions, and solid, reflecting walls in the z -direction. This box contains N particles whose motion is confined in the z -direction by a gravitational field of uniform acceleration, $\mathbf{g} = -g\hat{z}$, where \hat{z} is the unit vector along the z -axis (see figure 1). For the shear flows studied in the present work particles never touch the upper wall of the container due to the gravitational confinement.

In the following ways this setting is fundamentally different from that of the two-dimensional flows considered by Rahbari *et al.* (2010).

- (i) Rahbari *et al.* (2010) consider a flow at fixed density close to random close packing. In order to maintain constant density, particles passing each other in the flow require cooperative large-scale rearrangements of large portions of the system.

This is costly energetically, because it is accompanied by the breaking of a large number of capillary bridges.

- (ii) Conversely, in gravity-confined granular beds, particles can pass each other via a slight, local expansion of the bed in the vertical direction. Only a few capillary bridges must be ruptured in the resulting fixed-pressure setting, even though the density of the bed is always very close to random close packing.

2.1. Particle interactions

In the present study we consider monodisperse spheres of diameter d , in order to suppress any additional dynamics arising from different particle sizes. In fact, polydisperse beads, which are subject to small shearing forces, segregate according to their size (Schulz *et al.* 2003).

The dynamics in the simulation is calculated using a standard event-driven molecular-dynamics method which has been described in detail by Fingerle *et al.* (2008), Huang, Roeller & Herminghaus (2009), Roeller *et al.* (2009), Ulrich *et al.* (2009*a,b*) and Roeller (2010). For the sake of a self-contained exposition we only briefly summarize the particle interactions. Following Herminghaus (2005) the effect of particle adhesion due to the capillary bridges is modelled as follows.

- (i) Capillary interaction gives rise to pair forces between particles only.
- (ii) Unless particles are connected by a capillary bridge they feel no force when they approach each other.
- (iii) They collide elastically, and upon collision a capillary bridge is formed instantaneously. When the particles separate, this bridge gives rise to an attractive force which is modelled by placing the particles into a potential well with a depth E_{cb} , and a finite width s_{cb} .
- (iv) The liquid bridge ruptures at the critical rupture separation, s_{cb} . A rupture event is modelled by removing the potential well. Consequently the particles stop exerting a force on each other, until they touch once again.

In this manner the capillary bridge energy, E_{cb} , is dissipated whenever a capillary bridge is removed (i.e. ruptures) after a collision. Particle collisions, without bridge rupture, do not dissipate energy. They can, however, thermalize the particle velocities by redistributing kinetic energy from the ordered centre-of-mass motion into disordered motion. Henceforth, we shall refer to this as each particle's *thermal* degrees of freedom.

Work focusing on individual collisions (Davis, Rager & Good 2002; Antonyuk *et al.* 2009; Donahue *et al.* 2010*a,b*, 2012*a,b*; Gollwitzer *et al.* 2012) reports a multitude of features of particle collisions involving capillary interactions that cannot fully be captured by this model. On the other hand, the positions of phase boundaries of wet granular fluids appear to be universal in the sense that they only depend on E_{cb} and s_{cb} , and not on other details of the particle interaction (Huang *et al.* 2009). For computational convenience all simulations shown in the present paper therefore adopt a hysteretic square-well potential, i.e. we use an event-driven algorithm where the potential takes the form of a square-well with hysteresis as outlined in (i)–(iv).

2.2. Dimensionless units

Masses are measured in units of the particle mass, m , distances in units of the particle diameter, d , and the time unit is fixed by measuring forces in terms of mg . Non-dimensionalized quantities are denoted by a hat. Unless stated otherwise, the

system size is $\hat{L} \times 2\hat{L} \times \hat{H} = 60 \times 120 \times 7.5$, and the number of monodisperse particles is 4.39×10^4 , resulting in a filling height of $\hat{h} = 5.0$. Furthermore, the capillary interaction gives $\hat{E}_{cb} = 3/8$ and $\hat{s}_{cb} = 1/16$.

2.3. Shear flow and arrest

A shear flow is induced by applying a space-dependent external force field

$$\mathbf{F}_s(x) = F_s(x) \hat{\mathbf{y}} \quad \text{with } F_s(x) = F_{smax} \cos \frac{2\pi x}{L} \quad (2.1)$$

to the system (Hoover 1983; Schulz *et al.* 2003; Schulz & Schulz 2006; Rahbari *et al.* 2009, 2010), which accelerates particles along the $\hat{\mathbf{y}}$ -direction. The particles are initially homogeneously distributed within the system with a Gaussian velocity distribution of mean granular temperature $T_g/E_{cb} = 40.0$.

For external forces with an amplitude, F_{smax} , slightly larger than the critical forcing, F_{ex} , the system approaches a fluid flow whose local centre-of-mass velocity follows the external field. (The kinetic energy of states above the flow threshold gradually grows. Eventually, for time scales much larger than those studied here, this can lead to flow instabilities (see Roeller *et al.* 2009).) In figure 1(b) we illustrate such a system by visualizing a flow in a larger simulation box, where $\hat{L} = 100$ and $\hat{H} = 12.5$, accommodating a greater filling height of $\hat{h} \simeq 8.8$, and an external force only 11% above F_{ex} . In that situation shear bands form such that the capillary bridges in the region around $L_x/4$ and $3L_x/4$ are ruptured, while in the other parts the network of capillary bridges evolves only slowly. For shear forces smaller than F_{ex} the system eventually arrests in a solid state with a frozen network of nearest neighbours.

In passing we note that this arrest of flow is conceptually different from those jamming transitions where crowding and hard-core interactions prevent particles from passing each other, even at arbitrarily strong applied shear forces (Cates *et al.* 1998; Trappe *et al.* 2001; O'Hern *et al.* 2003; Drocco *et al.* 2005; Bi *et al.* 2011). This form of jamming is prevented here because the system can expand in the vertical direction where it is only bounded by gravity (see, for example Valverde, Quintanilla & Castellanos 2004 and references therein). Furthermore, the transition is also distinct from those observed in earlier studies on cohesive granular materials: we focus on the role of dissipation due to the hysteretic nature of capillary bridge ruptures, while previous studies (Trappe *et al.* 2001; Rognon *et al.* 2006, 2008) address conservative attractive forces. They implemented dissipation via grain friction and a restitution coefficient smaller than one (Rognon *et al.* 2006, 2008), or indirectly by treating the suspending fluid of attractive colloidal particles as an inert background (Trappe *et al.* 2001).

2.4. Measuring F_{ex}

The kinetic energy, E_y , of motion parallel to the driving shear force will serve as the order parameter to distinguish the dynamics. Rahbari *et al.* (2010) used the amplitude of the velocity profile in the direction of the external field (i.e. the amplitude of the velocity response in reaction to the applied force field, F_{smax}) as an order parameter. This has advantages when following the hysteresis loop of the response upon slowly decreasing and subsequently increasing F_{smax} . In the present study where we focus on the arrest of flow only, the kinetic energy, E_y , is a numerically stable and more easily accessible order parameter.

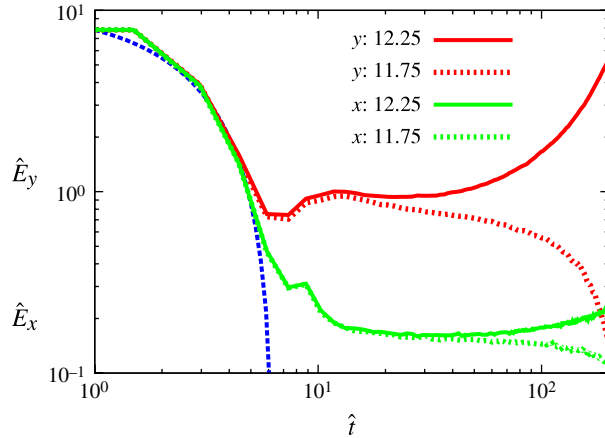


FIGURE 2. (Colour online) Time evolution of the kinetic energy, \hat{E}_y , of motion parallel to F_s (upper set of lines), and that in transverse direction, \hat{E}_x (lower set of lines) for a system of size $\hat{L} = 50$ driven by shear forces with amplitude $\hat{F}_{smax} \simeq 0.235$ (dotted lines) and 0.245 (solid lines), respectively. Initially all curves approximately follow the dynamics of free cooling (dashed line, see Ulrich *et al.* 2009b for the derivation) until the kinetic energy reaches values of the order of E_{cb} . Subsequently, the applied field is too weak to support sustained flow, and one encounters arrest at finite times into a state with no system-spanning flow (dotted line). For larger amplitudes of the force, the field injects a sufficient amount of energy into the system to permit sustained motion (solid lines). They eventually enter a state where the flow shows a rich time-dependent dynamics (cf. Roeller *et al.* 2009).

In figure 2 its time evolution is shown together with the kinetic energy, E_x , of the motion transverse to the external field. When started in a state with high kinetic energy, the fluid first cools down in a manner closely reminiscent of free cooling (Ulrich *et al.* 2009a,b). Starting at $\hat{t} \simeq 10$ it has cooled so far that the acceleration due to the external field becomes noticeable over the initial kinetic energy. Depending on whether the external field is stronger or weaker than a sharp critical value, \hat{F}_{ex} , the fluid either gains sufficient energy to remain in the fluid state forever, or it settles into the arrested state. The phase boundary, F_{ex} , is calculated as the mean value between the neighbouring values of shear forces, \hat{F}_{smax} , which approach different final states. For the data shown in figure 2 it is $\hat{F}_{ex} \simeq 0.240$.

The phase boundary hence corresponds to the smallest external force that still leads to sustained shear flow. We demonstrate in the following that the flow at this threshold corresponds to motion in a liquid state where the energy injected by the external field is exactly balanced by dissipation due to rupture of capillary bridges.

3. Fluidization point: two-dimensional model

In this section we discuss the power balance of the flow. Energy is injected into the kinetic energy of the particles due to their motion in the external force field. In a steady state this power is balanced by the energy dissipation rate due to the inelastic particle collisions. For external forces close to F_{ex} the granular temperature is small. Therefore, effects due to the thermal motion may be neglected, and the energy dissipation rate is dominated by the rupture of capillary bridges when particles pass each other in the flow field.

For all investigated systems the flow remains translationally invariant in the y -direction, in accordance with the symmetry of the forcing. Moreover, the density of the liquid cannot be distinguished from the random close packing density, ϕ_{rcp} , and the height of the layer is spatially uniform. Consequently, the number of particles, $n(x) dx$, in a thin rectangular cuboid of size $2L \times h \times dx$ aligned parallel to the external field takes a constant value, N/L , where N denotes the number of particles in the system and L the system size transverse to the flow. This finding is in line with the expectation that a flow breaking the symmetries of the system or noticeably expanding the bed would give rise to higher dissipation.

3.1. Energy injection rate

Let $v_y(x)$ denote the profile of the flow established when applying the critical force $F_s(x) = F_{smax} \cos(2\pi x/L) \doteq F_{ex} \cos(2\pi x/L)$. The input power that is injected by means of this external force acting on the particles is given by

$$\begin{aligned} \langle P_{forcing} \rangle &= \int_0^L v_y(x) F_s(x) n(x) dx \\ &= \frac{N F_{ex}}{L} \int_0^L v_y(x) \cos \frac{2\pi x}{L} dx. \end{aligned} \tag{3.1}$$

Up to the factor $N F_{ex}$ this amounts to the leading-order Fourier coefficient of the expansion of the velocity profile $v_y(x)$. Consequently, the injected power takes the form

$$\langle P_{forcing} \rangle = C_f N \Delta v_y F_{ex} \tag{3.2}$$

where Δv_y is the amplitude of the velocity field. Admissible values of C_f lie in the narrow range $0.5 < C_f < \pi/4$. The constant C_f takes the value 0.5 when the velocity profile is faithfully approximated by its first even harmonic, i.e. $v_y(x) \simeq \Delta v_y \cos(2\pi x/L)$, and $C_f = \pi/4 \simeq 0.785$ in the other extreme case of plug flow. Hence, C_f characterizes the shape of the velocity response to the applied external field.

3.2. Energy dissipation rate

For each particle the creeping flow enforces a change of neighbours (in the direction of the flow) with a rate $\dot{\gamma} = dv_y/dx$. Such a displacement results in an energy dissipation of $\dot{\gamma} \nu E_{cb}$ due to rupturing on average a number ν of capillary bridges per change of neighbours. The total power dissipated upon rupturing capillary bridges is thus given by

$$\langle P_{bridge} \rangle = \int_0^L n(x) \left| \frac{dv_y}{dx} \right| \nu E_{cb} dx. \tag{3.3}$$

For every L -periodic function $v_y(x)$ with a single local maximum per period, this integral yields

$$\langle P_{bridge} \rangle = \frac{4 N \Delta v_y}{L} \nu E_{cb}, \tag{3.4}$$

provided that $n(x) \equiv N/L$ is spatially uniform.

For the present system, rearrangements due to two particles passing each other are achieved by a slight vertical expansion of the particle bed. Assuming that there is no

height preference for the rearrangements, and that there are on average $h/2d$ particles in the column on top of the pair under consideration, a potential energy of

$$U = C_U \frac{h}{2d} mg \Delta h \quad (3.5)$$

is associated with the expansion. Here, C_U accounts for the number of columns to be lifted, and Δh to the expansion in height. Due to the frequent collisions in the dense bed the potential energy U is immediately dissipated into thermal degrees of freedom (i.e. the random component of the particle velocities) of the granular fluid, and therefore it is not just a one-off investment. Rather, work has to be done against gravity each time particles move past each other. Multiplying this energy with the frequency of particle passages, $4N\Delta v_y/L$ (as given by (3.4)), therefore provides a second contribution to the energy dissipation,

$$\langle P_{grav} \rangle = \frac{4N\Delta v_y}{L} U = \frac{4N\Delta v_y}{L} C_U \frac{\Delta h}{2d} mgh. \quad (3.6)$$

3.3. Predicting the critical force \hat{F}_{ex}

Assuming that bridge rupture occurs only in the plane parallel to the applied force, the effect of the third dimension is then only to provide an additional energy sink due to gravity, $\langle P_{grav} \rangle$. Therefore, in a steady state the total dissipation rate, due to rupturing bridges and relaxation of U into thermal degrees of freedom, has to balance the input power. We hence obtain

$$\begin{aligned} \langle P_{forcing} \rangle &= \langle P_{bridge} \rangle + \langle P_{grav} \rangle \\ \Leftrightarrow F_{ex} L &= a E_{cb} + b mgh \\ \Leftrightarrow \hat{F}_{ex} \hat{L} &= a \hat{E}_{cb} + b \hat{h}, \end{aligned} \quad (3.7a)$$

$$\text{with } a = \frac{4\nu}{C_f} \quad (3.7b)$$

$$b = \frac{2C_U \Delta \hat{h}}{C_f}. \quad (3.7c)$$

At this point, it is worth pointing out that the flow's response to the external force field is characterized by its amplitude, Δv_y , and the parameter, C_f , which characterizes the shape of the velocity response. The amplitude-dependence, Δv_y , cancels in the power balance. In the worst case, the parameter C_f can vary by no more than a factor of 1.6. Furthermore, for external forcing close to \hat{F}_{ex} the variability is expected to be even smaller. Hence, one expects that \hat{F}_{ex} is well-approximated by (3.7) under the assumption that C_f is a constant of order unity. Thus, it is not necessary to determine C_f by calculating it from the flow directly.

The coefficient a characterizes the mean number of capillary bridges ruptured in the flow as particles pass each other. Likewise C_U counts how many rows of particles are lifted when the particles pass each other. As a consequence, $b mgh$ is the average amount of work done against gravity in the flow per unit time.

We hence predict that \hat{F}_{ex} is inversely proportional to the system size \hat{L} , and that $\hat{F}_{ex} \hat{L}$ is a linear function of \hat{E}_{cb} and the filling height \hat{h} . In the following section we compare these predictions to the results of the molecular-dynamics simulations.

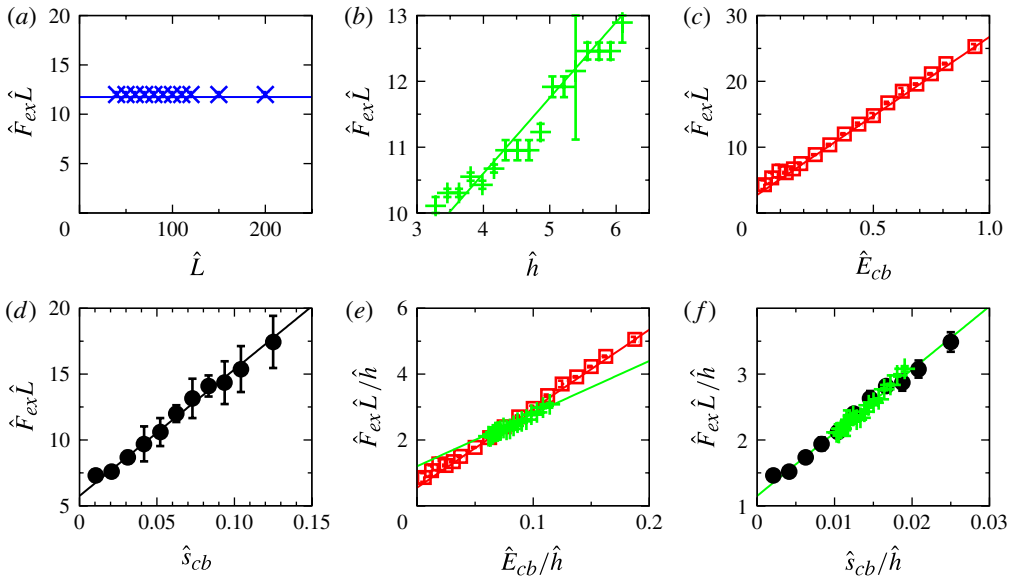


FIGURE 3. (Colour online) The parameter dependence of the critical driving forces, \hat{F}_{ex} , separating regions that lead to either solid or fluidized behaviour. The symbols indicate the phase boundary between the two phases, and solid lines are the theoretical predictions described in the main text. For most of the data points the numerical error in the phase boundary is smaller than the size of the symbol. (a–d) The phase boundary between the solid and the fluidized state upon varying different parameters: (a) system size, \hat{L} , (b) filling height \hat{h} , (c) dissipated energy, \hat{E}_{cb} , and (d) critical rupture separation, \hat{s}_{cb} . In (e) $\hat{F}_{ex}\hat{L}/\hat{h}$ is plotted as a function of \hat{E}_{cb}/\hat{h} in order to demonstrate that the data of (b) and (c) are not compatible with the prediction, (3.7). (f) A collapse of the data of (b) and (d), when $\hat{F}_{ex}\hat{L}/\hat{h}$ is plotted as a function \hat{s}_{cb}/\hat{h} in order to demonstrate that \hat{s}_{cb} and \hat{h} , rather than \hat{E}_{cb} and \hat{h} may be considered independent parameters to predict $\hat{F}_{ex}\hat{L}$. The method for performing the simulations is discussed in the text.

4. Comparison to numerical data

In figure 3(a–d) we explore the dependence of \hat{F}_{ex} on the systems size, L , the filling height, h , the dissipated energy, E_{cb} , and the rupture length, \hat{s}_{cb} . Plotting \hat{F}_{ex} as a function of the respective parameters provides sections through the phase diagram: there is sustained flow for values of \hat{F}_s larger than \hat{F}_{ex} and flow is arrested for smaller external forces.

4.1. Parameter dependence of \hat{F}_{ex}

(a) The system size \hat{L} was varied whilst keeping the aspect ratio of the container constant at $L_y/L_x = 2$. At the same time the average particle number density was kept constant at $\phi = 0.43$ which means that the number of particles is changing in order to provide a fixed filling height, $\hat{h} \simeq 5$. As expected from (3.7) the value of $\hat{F}_{ex}\hat{L}$ is constant. We find that $\hat{F}_{ex}\hat{L} \simeq 12$ for fixed $\hat{E}_{cb} = 0.375$ and $\hat{h} \simeq 5$ (figure 3a).

(b) The filling height, \hat{h} , was varied by changing the number of particles in the system whilst keeping the geometry of the simulation volume and particle interactions fixed. The filling height is estimated as the filling height in the solid state when

assuming random close packing. As predicted by (3.7) the dependence of $\hat{F}_{ex}\hat{L}$ on \hat{h} for a fixed \hat{E}_{cb} is linear. In the simulations we find

$$\hat{F}_{ex}\hat{L} \simeq 6.0 + 1.2\hat{h} \quad (4.1)$$

for $\hat{E}_{cb} = 0.375$ (figure 3b).

(c) Whilst varying the capillary bridge energy, E_{cb} , the rupture separation, $\hat{s}_{cb} = 1/16$, filling height, $\hat{h} \simeq 5$, and the system size, $\hat{L} = 60$, were kept constant. Figure 3(c) shows the expected linear dependence of $\hat{F}_{ex}\hat{L}$ on \hat{E}_{cb} ,

$$\hat{F}_{ex}\hat{L} \simeq 24\hat{E}_{cb} + 2.8. \quad (4.2)$$

Central to the assertion of linear dependence is that C_f takes a constant value close to arrest. The slight deviation from the linear fit for small \hat{E}_{cb} expresses a slight increase of the deviation of the velocity profile from a cosine profile.

(d) The critical rupture separation, s_{cb} , was varied for a fixed aspect ratio of width versus depth of the potential well, i.e. E_{cb} was varied together with s_{cb} at a fixed ratio of $R \equiv E_{cb}/s_{cb} = 6.0$. System size and filling height were fixed to $\hat{L} = 60$ and $\hat{h} = 5$, respectively. The resulting linear dependence

$$\hat{F}_{ex}\hat{L} \simeq 16R\hat{s}_{cb} + 6.0 \quad (4.3)$$

is shown in figure 3(d).

4.2. Consistency checks: effects of the third dimension

Merely finding linear dependences of \hat{F}_{ex} on \hat{h} , \hat{E}_{cb} and \hat{s}_{cb} is not sufficient to show that (3.7) faithfully describes the arrest of flow. One also has to verify that the linear functions are mutually consistent for all sections through the phase diagram.

(e) In order to compare (4.1) and (4.2), their respective y-intercepts need to be expressed in terms of the quantity held constant in (b) and (c). The y-intercept of (4.1) may be written as $6.0 \simeq 16\hat{E}_{cb}$ given that $\hat{E}_{cb} = 0.375$. Whereas the y-intercept of (4.2) can be written as $2.8 \simeq 0.56\hat{h}$ for $\hat{h} = 5$. This gives two linear equations,

$$\hat{F}_{ex}\hat{L} \simeq 16\hat{E}_{cb} + 1.2\hat{h} \quad \text{according to (4.1),} \quad (4.4a)$$

$$\hat{F}_{ex}\hat{L} \simeq 24\hat{E}_{cb} + 0.56\hat{h} \quad \text{according to (4.2),} \quad (4.4b)$$

that must hold simultaneously if (3.7) is an accurate model. Plotting $\hat{F}_{ex}\hat{L}/\hat{h}$ versus \hat{E}_{cb}/\hat{h} in figure 3(e) shows that this is clearly not the case. Consequentially the data shown in figure 3(b,c) lie on different straight lines. It is not admissible to interpret (3.7a) as a linear relation with constant coefficients a and b , and \hat{E}_{cb} and \hat{h} as independent variables.

(f) In order to provide a physical interpretation of the origin of this deviation, we note that the data shown in figures 3(d) and 3(b) are compatible. Equation (4.3) is commensurate with (4.1) since the latter has a y-intercept of $6.0 = 16\hat{E}_{cb} = 16R\hat{s}_{cb}$ with $R = 6.0$ and $\hat{s}_{cb} = 1/16$, and since the y-intercept of (4.3) is $6.0 = 1.2\hat{h}$ with $\hat{h} = 5.0$.

In the following we show that a consistent description of the numerical data can only be achieved by assuming that a has a weak, linear dependence on \hat{h} .

Equation (3.7) is consistent with the numerical data when taking into account a monotonic increase of the number of bridge ruptures for increasing h/s_{cb} . After

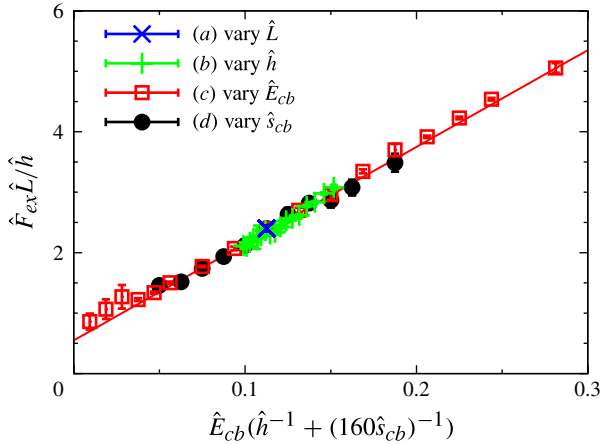


FIGURE 4. (Colour online) The solid line shows our theoretical prediction, (5.1) involving only three free parameters \tilde{a} , \tilde{b} , and $\tilde{\chi}$ whose values can also explicitly be calculated. It provides a master plot incorporating all data shown in the different panels of figure 3. The dependence of the critical force F_{ex} on the system size, \hat{L} , the filling height, \hat{h} , the energy dissipated upon rupturing capillary bridges, \hat{E}_{cb} , and the critical rupture separation, \hat{s}_{cb} , is faithfully described. The data points referring to different system size are so close that they all lie on top of each other in this representation.

all, swapping events also lead to rupturing bridges along the sides of the vertically displaced column of particles on top of the considered site.

5. Fluidization point: three-dimensional model and data collapse

The likelihood of rupturing bridges in the vertical direction can be derived from the disparity between (4.3) and (4.2). They can only be consistent if the y-intercept of (4.3) comprises a contribution proportional to R , and if the slopes are adjusted accordingly, i.e. by decomposing the y-intercept as $6.0 = 1.2\hat{h} \simeq (0.55 + R/10)\hat{h}$ with $\hat{h} = 5$ and $R = 6.0$. Observing that $R \equiv E_{cb}/s_{cb}$ this provides an improved prediction

$$\hat{F}_{ex}\hat{L} \simeq \left(1 + \tilde{\chi} \frac{\hat{h}}{\hat{s}_{cb}}\right) \tilde{a}\hat{E}_{cb} + \tilde{b}\hat{h}. \tag{5.1a}$$

The agreement of all of our numerical data with this prediction is demonstrated in figure 4. It shows a master plot where all data shown in figure 3 collapse on a single line, (5.1a) with coefficients

$$\tilde{a} \simeq 16 \quad \text{bridge ruptures,} \tag{5.1b}$$

$$\tilde{b} \simeq 0.55 \quad \text{flow dilation,} \tag{5.1c}$$

$$\tilde{\chi} \simeq 1/160 \quad \text{out-of-plane bridge ruptures.} \tag{5.1d}$$

A priori, it is not clear whether these values comply with their physical interpretation. As a final step of the data analysis, we check our findings by estimating the expected values of the parameters \tilde{a} , \tilde{b} and $\tilde{\chi}$.

5.1. Determination of \tilde{a}

In view of (3.7b) the parameter a is related to the number, ν , of capillary bridge ruptures in every particle exchange

$$a = \frac{4\nu}{C_f} \simeq 8\nu, \quad (5.2)$$

where we used the estimate $C_f \simeq 0.5$, as argued upon introducing this constant in (3.2). Moreover, in order to take into account the correction term for the height dependence introduced in (5.1) another factor $1 + \hat{h}/160\hat{s}_{cb}$ must also be considered. For the standard choice of parameters $\hat{h} = 5$ and $\hat{s}_{cb} = 1/16$ we hence find

$$\tilde{a} = \frac{4\nu}{C_f} \left(1 + \frac{\hat{h}}{160\hat{s}_{cb}} \right)^{-1} \simeq \frac{16}{3}\nu. \quad (5.3)$$

Finally, in a granular bed that is expanding to allow particles to pass each other the number ν of rupture events must be larger than 1, but still small. For $\nu = 3$ we hence recover the value $\tilde{a} = 16$ reported in (5.1b).

5.2. Determination of \tilde{b}

In order to see that the value for $b \simeq 0.55$ is also reasonable, we observe that subsequent rows of spheres in a close-packed structure are separated by a height distance $\hat{h}_{cp} = \sqrt{2/3} \simeq 0.816$ and that the saddle that has to be passed to roll from one minimum to a nearby minimum is at height $\hat{h}_{saddle} = \sqrt{3}/2 \simeq 0.866$. The minimum expansion in height to move over the potential landscape set up by the layers below is therefore of the order of $\Delta\hat{h} \simeq \hat{h}_{saddle} - \hat{h}_{cp} \simeq 0.05$. Potential wells in a disordered, only slightly expanded random packing, will still be of the same order of magnitude. Based on this estimate, on $C_f \simeq 0.5$, and on (3.7c) the number of columns, C_U , lifted in a swapping event amounts to

$$C_U \simeq 0.55 \frac{C_f}{2\Delta\hat{h}} \simeq 2.8. \quad (5.4)$$

Lifting a small number of columns gives plausibility to $b \simeq 0.55$.

5.3. Determination of $\tilde{\chi}$

In order to gain insight into the order of magnitude of $\tilde{\chi}$ we note that the lifted column needs to rupture bonds all along its walls. Hence, ν is not merely dependent on its cross-section, as implied by assuming ν to be independent of \hat{h} . The number of bonds that are broken is then expected to scale linearly with column height and inversely proportional to \hat{s}_{cb} . After all, bonds are allowed to stretch to a finite length \hat{s}_{cb} , and the larger \hat{s}_{cb} the lower the likelihood that the dilation requires a given bond (along the vertical walls of the pile of particles displaced vertically) to be broken. This leads to an additional number $\tilde{\chi}\nu\hat{h}/\hat{s}_{cb}$ of bonds broken per column. As we saw above, it increases the number of bond ruptures by $\sim 50\%$ which seems reasonable in a system with a packing height of only five layers and a rupture separation, $\hat{s}_{cb} = 1/16 = 0.065$ that is larger than the average height displacement, $\Delta\hat{h} = 0.05$, of the column. After all, in such a situation only pre-stretched bonds are likely to rupture. Keeping this in mind, the small value of $\tilde{\chi}$ may be understood as a result of incorporating a factor of $\Delta\hat{h}$ and a probability of $\sim 1/4$ to encounter a pre-stretched

bond in a layer of a column that is vertically displaced. In this interpretation the average number of layers in the column is $\hat{h}/2$.

6. Summary and outlook

The present study substantiates the finding that the transition from a fluidized to an arrested state in wet granular matter arises when the dissipation rate due to the rupture of capillary bridges in the shear flow can no longer be balanced by the power injection from the external field. Earlier work (Rahbari *et al.* 2010) showed that this approach provides a comprehensive understanding of the transition in settings where the density is fixed by a confining box. The present work addressed the flow of a bed kept at constant pressure by confining it in the vertical direction by a gravitational field. Just above the transition the flow is reminiscent of a slow plastic flow of the bed in the direction of the applied field: the bed expands only minimally in the vertical direction, and gravity keeps density, filling height, and pressure to values observed in an arrested packing. Also, for this gravitationally confined wet granular flow the power balance provides an accurate prediction, (5.1), of the critical force at which the flow ceases. This is demonstrated by a master plot, figure 4, showing a collapse of all numerical data obtained by varying four different characteristics of the system: the system size, the filling height, as well as the strength and critical rupture separation of capillary bridges. Our data collapse suggests that the prediction of the flow threshold involves only three constants characterizing the types of dissipative events:

- (i) When the granular flow is confined by gravity, typically only 2–3 capillary bridges are ruptured upon swapping neighbouring particles moving with slightly different speed in the direction of the external forcing. This is a striking difference to wall-bounded flows (Rahbari *et al.* 2010) where this number diverges when the density approaches close packing.
- (ii) In a gravity-confined granular bed the effortless passing of the particles is facilitated by a slight expansion of the granular bed where 2–3 columns of particles are lifted by a small amount to let the particles pass between neighbouring potential wells arising from the corrugations formed by the layer below. The associated potential energy is also dissipated.
- (iii) With a small probability additional capillary bridges are broken due to the slight expansions in vertical direction.

The most remarkable finding of our study is that the critical force F_{ex} can be determined from the forcing alone. No details of the flow's response are required to predict whether the flow will arrest. F_{ex} can be calculated without specifying the hydrodynamic equations of the flow and determining their solution. We therefore conclude that the approach of balancing the energy input rate (due to the external force inducing the flow) and the dissipation rate (due to the rupture of capillary bridges, when particles move past each other) provides a powerful framework to study the arrest of flow in wet granular materials. It provides a universal method to predict the threshold for the arrest of flow.

Acknowledgements

We are indebted to M. Brinkmann, K. Daniels, W. Losert and M. Schröter for stimulating discussion. J.B., S.H., and J.V. gratefully acknowledge financial support by BP Exploration Operating Company Ltd.

REFERENCES

- ANDREOTTI, B., DAERR, A. & DOUADY, S. 2002 Scaling laws in granular flows down a rough plane. *Phys. Fluids* **14** (1), 415.
- ANDREOTTI, B. & DOUADY, S. 2001 Selection of velocity profile and flow depth in granular flows. *Phys. Rev. E* **63** (3), 031305.
- ANTONYUK, S., HEINRICH, S., DEEN, N. & KUIPERS, H. 2009 Influence of liquid layers on energy absorption during particle impact. *Particuology* **7** (4), 245–259.
- ARANSON, I. S. & TSIMRING, L. S. 2006 Patterns and collective behaviour in granular media: theoretical concepts. *Rev. Mod. Phys.* **78** (2), 641.
- BERARDI, C. R., BARROS, K., DOUGLAS, J. F. & LOSERT, W. 2010 Direct observation of stringlike collective motion in a two-dimensional driven granular fluid. *Phys. Rev. E* **81** (4), 041301.
- BI, D., ZHANG, J., CHAKRABORTY, B. & BEHRINGER, R. P. 2011 Jamming by shear. *Nature* **480** (7377), 355–358.
- BORZSONYI, T. & ECKE, R. E. 2007 Flow rule of dense granular flows down a rough incline. *Phys. Rev. E* **76** (3), 031301.
- CATES, M. E., WITTMER, J. P., BOUCHAUD, J.-P. & CLAUDIN, P. 1998 Jamming, force chains, and fragile matter. *Phys. Rev. Lett.* **81** (9), 1841–1844.
- DAVIS, R. H., RAGER, D. A. & GOOD, B. T. 2002 Elastohydrodynamic rebound of spheres from coated surfaces. *J. Fluid Mech.* **468**, 107–119.
- DONAHUE, C. M., BREWER, W. M., DAVIS, R. H. & HRENYA, C. M. 2012a Agglomeration and de-agglomeration of rotating wet doublets. *J. Fluid Mech.* **708**, 128–148.
- DONAHUE, C. M., DAVIS, R. H., KANTAK, A. A. & HRENYA, C. M. 2012b Mechanisms for agglomeration and deagglomeration following oblique collisions of wet particles. *Phys. Rev. E* **86**, 021303.
- DONAHUE, C. M., HRENYA, C. M. & DAVIS, R. H. 2010a Stokes' cradle: Newton's cradle with liquid coating. *Phys. Rev. Lett.* **105**, 034501.
- DONAHUE, C. M., HRENYA, C. M., DAVIS, R. H., NAKAGAWA, K. J., ZELINSKAYA, A. P. & JOSEPH, G. G. 2010b Stokes' cradle: normal three-body collisions between wetted particles. *J. Fluid Mech.* **650**, 479–504.
- DROCCO, J. A., HASTINGS, M. B., OLSON REICHHARDT, C. J. & REICHHARDT, C. 2005 Multiscaling at point j : jamming is a critical phenomenon. *Phys. Rev. Lett.* **95** (8), 088001.
- RAHBARI, S. H. E., VOLLMER, J., HERMINGHAUS, S. & BRINKMANN, M. 2009 A response function perspective on yielding of wet granular matter. *Europhys. Lett.* **87**, 14002.
- FINGERLE, A., ROELLER, K., HUANG, K. & HERMINGHAUS, S. 2008 Phase transitions far from equilibrium in wet granular matter. *New J. Phys.* **10** (5), 053020.
- FORTERRE, Y. & POULIQUEN, O. 2008 Flows of dense granular media. *Annu. Rev. Fluid Mech.* **40**, 1–24.
- GDR MIDI, 2004 On dense granular flows. *Eur. Phys. J. E* **14**, 341–365.
- GOLLWITZER, F., REHBERG, I., KRUELLE, C. A. & HUANG, K. 2012 Coefficient of restitution for wet particles. *Phys. Rev. E* **86**, 011303.
- VAN HECKE, M. 2010 Jamming of soft particles: geometry, mechanics, scaling and isostaticity. *J. Phys.: Condensed Matter* **22** (3), 033101.
- HERMINGHAUS, S. 2005 Dynamics of wet granular matter. *Adv. Phys.* **54** (3), 221–261.
- HOOVER, W. G. 1983 Nonequilibrium molecular dynamics. *Annu. Rev. Phys. Chem.* **34** (1), 103–127.
- HUANG, K., ROELLER, K. & HERMINGHAUS, S. 2009 Universal and non-universal aspects of wet granular matter under vertical vibrations. *Eur. Phys. J. Special Topics* **179**, 25–32.
- JAEGER, H. M., NAGEL, S. R. & BEHRINGER, R. P. 1996 Granular solids, liquids, and gases. *Rev. Mod. Phys.* **68** (4), 1259–1273.
- JOP, P., FORTERRE, Y. & POULIQUEN, O. 2006 A constitutive law for dense granular flows. *Nature* **441**, 727–730.
- KADANOFF, L. P. 1999 Built upon sand: theoretical ideas inspired by granular flows. *Rev. Mod. Phys.* **71** (1), 435–444.

- KANTAK, A. A., HRENYA, C. M. & DAVIS, R. H. 2009 Initial rates of aggregation for dilute, granular flows of wet particles. *Phys. Fluids* **21**, 023301.
- LIAO, C.-C. & HSIAU, S.-S. 2010 Experimental analysis of dynamic properties in wet sheared granular matter. *Powder Technol.* **197** (3), 222–229.
- LOIS, G., BLAWDZIEWICZ, J. & O’HERN, C. S. 2007 Jamming in attractive granular media. *Proc. Appl. Maths. Mech.* **7** (1), 1090605–1090606.
- LOIS, G., BLAWDZIEWICZ, J. & O’HERN, C. S. 2008 Jamming transition and new percolation universality classes in particulate systems with attraction. *Phys. Rev. Lett.* **100**, 028001.
- LOIS, G., ZHANG, J., MAJMUDAR, T. S., HENKES, S., CHAKRABORTY, B., O’HERN, C. S. & BEHRINGER, R. P. 2009 Stress correlations in granular materials: an entropic formulation. *Phys. Rev. E* **80**, 060303.
- LUDING, S. 2009 Towards dense, realistic granular media in 2d. *Nonlinearity* **22** (12), R101–R146.
- MITARAI, N. & NORI, F. 2006 Wet granular materials. *Adv. Phys.* **55** (1–2), 1–45.
- O’HERN, C. S., SILBERT, L. E., LIU, A. J. & NAGEL, S. R. 2003 Jamming at zero temperature and zero applied stress: the epitome of disorder. *Phys. Rev. E* **68** (1), 011306.
- PITTOIS, O., MOUCHERONT, P. & CHATEAU, X. 2000 Liquid bridge between two moving spheres: an experimental study of viscosity effects. *J. Colloid Interface Sci.* **231**, 26–31.
- QUARTIER, L., ANDREOTTI, B., DOUADY, S. & DAERR, A. 2000 Dynamics of a grain on a sandpile model. *Phys. Rev. E* **62** (6), 8299.
- RAHBARI, S. H. E., VOLLMER, J., HERMINGHAUS, S. & BRINKMANN, M. 2009 A response function perspective on yielding of wet granular matter. *Europhys. Lett.* **87** (1), 14002.
- RAHBARI, S. H. E., VOLLMER, J., HERMINGHAUS, S. & BRINKMANN, M. 2010 Fluidization of wet granulates under shear. *Phys. Rev. E* **82** (6), 061305.
- REMY, B., KHINAST, J. G. & GLASSER, B. J. 2012. Wet granular flows in a bladed mixer: experiments and simulations of monodisperse spheres, *AIChE J.* (submitted).
- REN, J., DIKSMAN, J. A. & BEHRINGER, R. P. 2011 Linear shear in a model granular system. *CHAOS*.
- ROELLER, K. 2010. Numerical simulations of wet granular matter. PhD thesis, University Goettingen.
- ROELLER, K., VOLLMER, J. & HERMINGHAUS, S. 2009 Unstable Kolmogorov flow in granular matter. *CHAOS* **19** (4), 041106.
- ROGNON, P. G., ROUX, J.-N., NAAÏM, M. & CHEVOIR, F. 2008 Dense flows of cohesive granular materials. *J. Fluid Mech.* **596**, 21–47.
- ROGNON, P. G., ROUX, J.-N., WOLF, D., NAAÏM, M. & CHEVOIR, F. 2006 Rheophysics of cohesive granular materials. *Eur. Phys. Lett.* **74** (4), 644.
- SCHALL, P. & VAN HECKE, M. 2010 Shear bands in matter with granularity. *Annu. Rev. Fluid Mech.* **42** (1), 67–88.
- SCHULZ, B. M. & SCHULZ, M. 2006 The dynamics of wet granular matter. *J. Non-Crystalline Solids* **352** (42–49), 4877–4879.
- SCHULZ, M., SCHULZ, B. M. & HERMINGHAUS, S. 2003 Shear-induced solid–fluid transition in a wet granular medium. *Phys. Rev. E* **67** (5), 052301.
- SILBERT, L. E., ERTAŞ, D., GREST, G. S., HALSEY, T. C., LEVINE, D. & PLIMPTON, S. J. 2001 Granular flow down an inclined plane: Bagnold scaling and rheology. *Phys. Rev. E* **64** (5), 051302.
- SLOTTERBACK, S., MAILMAN, M., RONASZEGI, K., VAN HECKE, M., GIRVAN, M. & LOSERT, W. 2012 Onset of irreversibility in cyclic shear of granular packings. *Phys. Rev. E* **85** (2), 021309.
- TORDESILLAS, A., LIN, Q., ZHANG, J., BEHRINGER, R. P. & SHI, J. 2011 Structural stability and jamming of self-organized cluster conformations in dense granular materials. *J. Mech. Phys. Solids* **59**, 265–296.
- TRAPPE, V., PRASAD, V., CIPELLETTI, L., SEGRE, P. N. & WEITZ, D. A. 2001 Jamming phase diagram for attractive particles. *Nature* **411**, 772–775.
- ULRICH, S., ASPELMEIER, T., ROELLER, K., FINGERLE, A., HERMINGHAUS, S. & ZIPPELIUS, A. 2009a Cooling and aggregation in wet granulates. *Phys. Rev. Lett.* **102** (14), 148002.

- ULRICH, S., ASPELMEIER, T., ZIPPELIUS, A., ROELLER, K., FINGERLE, A. & HERMINGHAUS, S. 2009*b* Dilute wet granular particles: nonequilibrium dynamics and structure formation. *Phys. Rev. E* **80** (3), 031306.
- UTTER, B. & BEHRINGER, R. P. 2008 Experimental measures of affine and nonaffine deformation in granular shear. *Phys. Rev. Lett.* **100**, 208302.
- VALVERDE, J. M., QUINTANILLA, M. A. S. & CASTELLANOS, A. 2004 Jamming threshold of dry fine powders. *Phys. Rev. Lett.* **92** (25), 258303.
- ZHANG, J., MAJMUDAR, T. S., TORDESILLAS, A. & BEHRINGER, R. P. 2010 Statistical properties of a 2D granular material subjected to cyclic shear. *Granul. Matt.* **12** (2), 159–172.